

# Quartz fiber calorimetry and calorimeters \*

G. Mavromanolakis \*\*

*University of Cambridge, Department of Physics  
Cavendish Laboratory, High Energy Physics Group  
Madingley Road, Cambridge, CB3 0HE, UK*

Quartz fiber calorimetry is a technique the signal generation mechanism of which is based on the Cherenkov effect. In this article we try to give a comprehensive overview of the subject. We start with a general introduction to calorimetry where the basic elements that characterize the development of electromagnetic and hadronic showers are discussed. Then we describe in detail the operation principle and the properties of calorimeters equipped with quartz fibers. The main advantages of this type of calorimeters are the radiation hardness, the fast response and the compact detector dimensions, features that derive from the quartz material and the specific mechanism of operation. A section is devoted to presenting the quartz fiber calorimeters that have been built or planned to in various experiments to operate as centrality detectors, trigger detectors, luminosity monitors or general purpose very forward calorimeters.

## Contents

<b>1</b>	<b>Introduction to calorimetry</b>	<b>3</b>
1.1	Electromagnetic shower development . . . . .	3
1.2	Hadronic shower development . . . . .	6
1.3	Energy resolution of calorimetric measurement . . . . .	7
<b>2</b>	<b>Quartz fiber calorimetry</b>	<b>10</b>
2.1	Motivation . . . . .	10
2.2	Principle of operation and Cherenkov effect . . . . .	10
2.3	Light propagation in optical fibers . . . . .	12

---

\* Material based on notes and seminars given at University of Athens, Department of Physics

\*\* email: gmavroma@hep.phy.cam.ac.uk or gmavroma@mail.cern.ch

2.4	Quartz optical fibers . . . . .	14
2.5	Basic properties of quartz fiber calorimeters . . . . .	15
<b>3</b>	<b>Quartz fiber calorimeters</b>	<b>16</b>
3.1	The Zero Degree calorimeter for the NA50 experiment at CERN-SPS . . . . .	19
3.2	The Very Forward calorimeter for the CMS experiment at CERN-LHC . . . . .	19
3.3	The Zero Degree calorimeters for the ALICE experiment at CERN-LHC . . . . .	19
3.4	The Very Forward EM calorimeter for the NA52 experiment at CERN-SPS . . . . .	20
3.5	The Zero Degree calorimeters of the experiments at BNL-RHIC . . . . .	20
3.6	The Very Forward EM calorimeter for the H1 experiment at DESY-HERA . . . . .	21
3.7	The CASTOR calorimeter for the CERN-LHC . . . . .	21
3.8	Other calorimeters . . . . .	21
<b>4</b>	<b>Summary</b>	<b>22</b>
	<b>References</b>	<b>31</b>

# 1 Introduction to calorimetry

Calorimetry comprises the experimental methods one develops to perform energy measurement. A calorimeter [1]-[6] is a detector, literally a block of matter with proper instrumentation, which measures the energy of incident particles. Its characteristic feature is that the resolution of the energy measurement improves with energy, while the size of the detector scales logarithmically with it. Also of importance is the fact that a calorimeter is a detector which is sensitive to both charged and neutral incident particles. Depending on appropriate construction, calorimeters can also provide position measurement and particle identification in addition to energy measurement. The signal generation mechanism in a calorimeter is as follows: the incident particle interacts inside the calorimeter volume and initiates a shower of secondary particles, the shower develops and its products generate signal by passing through the sensitive material of the calorimeter. The operation principle of the majority of calorimeters is based on the  $dE/dx$  technique, i.e. the signal depends on the energy deposited by the shower particles in the sensitive material, and is generated by scintillation or ionization. The signal can be light, for calorimeters with scintillators, or ionization charge, for those with gaseous or semiconductive sensitive material. Calorimeters with a different principle of operation are those composed of lead glass or quartz fibers. For these, the signal generation mechanism is based on the Cherenkov effect.

Calorimeters can be distinguished between electromagnetic and hadronic, whether they are designed to measure the energy of incident electrons, positrons and photons, or hadrons, respectively. They are also categorized in homogeneous and sampling calorimeters, depending on their construction. In a homogeneous calorimeter, the whole volume is considered sensitive, i.e. shower production and development and signal generation and collection occur at the same material. The main advantage of this type of calorimeters is their excellent performance with respect to energy resolution. A sampling calorimeter is composed of two different materials. A passive material, the absorber, where the shower develops, and the sensitive or active material where the signal is produced and collected. The absorber is usually copper, steel, lead or other dense metal. The sensitive material, that can be scintillator plates, gas tubes or silicon layers, is placed between consecutive absorber layers (“sandwich” structure) or is uniformly distributed inside the absorber volume, as in the case of scintillation tiles or fibers (“spaghetti” structure). Sampling calorimeters have worse energy resolution because the statistical fluctuations in production and collection of their signal are significantly larger compared to homogeneous ones. However, they cost less, have compact size and are the only practical means one can use to measure the energy of hadrons.

## 1.1 Electromagnetic shower development

For energies above 1 GeV, electrons and positrons lose energy through bremsstrahlung, and photons through pair production [1]-[10]. The secondary particles produced interact through the same processes and a shower develops inside the calorimeter. For

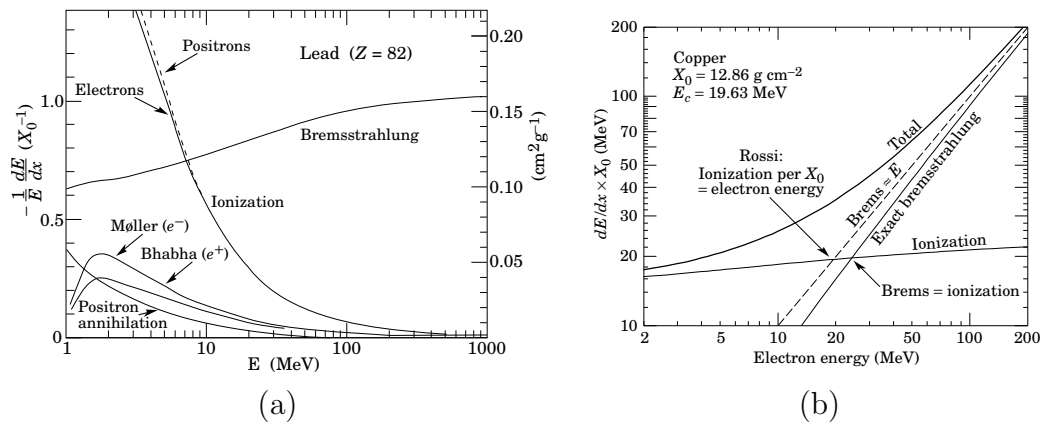


Figure 1: (a) relative energy loss per unit length ( $\frac{1}{E} \frac{dE}{dx}$ ) in lead for different processes as a function of electron or positron energy, (b) energy loss per unit length from ionization and bremsstrahlung as a function of electron energy (in copper). Both forms of defining  $E_c$  are shown, according to  $(\frac{dE}{dx})_{ion} = (\frac{dE}{dx})_{brem}$  or  $(\frac{dE}{dx})_{ion} = \frac{E_c}{X_0}$ .

lower energies ( $E \lesssim 10 \text{ MeV}$ ) electrons and positrons interact with matter and lose energy mainly through ionization of the atoms of the detector. Additional processes such as bremsstrahlung, Moller scattering, Bhabha scattering or positron annihilation do not contribute significantly to energy loss, as shown in fig. 1(a) [10]. The shower development ceases when energy loss from ionization is greater than that from bremsstrahlung. The energy loss per unit length from ionization is practically constant, since it depends logarithmically on electron or positron energy,  $|dE/dx|_{ion} \propto \ln E$ , in contrast to energy loss from bremsstrahlung which shows linear dependence on energy,  $|dE/dx|_{brem} \propto E$  (fig. 1(b) [10]). We define *critical energy*,  $E_c$ , as the energy at which the loss rates from ionization and from bremsstrahlung become equal. The critical energy is a crucial parameter which characterizes the material of a calorimeter. It is well approximated by  $E_c \approx 800/(Z + 1.2)$ . Better representation of experimental results, as far as transverse shower development is concerned, can be achieved by using the following approximation [10]

$$E_c = \frac{610}{Z + 1.24} \text{ MeV, for liquids or solids} \quad (1)$$

$$E_c = \frac{710}{Z + 0.92} \text{ MeV, for gases} \quad (2)$$

where  $Z$  is the atomic number of material.

The *radiation length*,  $X_0$ , is another characteristic quantity, which is related to the longitudinal development of electromagnetic showers. It is defined as the mean distance that an electron traverses to lose  $(1 - 1/e)$  of its energy by bremsstrahlung. It is approximately  $X_0 \approx 180 \cdot A/Z^2$  (in  $\text{gr/cm}^2$ ), where  $A$ ,  $Z$  are mass and atomic numbers of material, respectively,

$$X_0 = \frac{716.4 \cdot A}{Z(Z + 1) \cdot \ln(287/\sqrt{Z})} \text{ gr/cm}^2 \quad (3)$$

For a photon, the mean distance that it travels before it converts to a  $e^-e^+$  pair with probability  $(1 - 1/e)$  is equal to  $\frac{9}{7}X_0$ .

The mean longitudinal profile of the energy deposition of a shower, or equivalently the longitudinal distribution of signal production, can be described by a  $\Gamma$ -distribution function [1, 5, 10],

$$\frac{dE}{dt} = E \cdot b \cdot \frac{(bt)^{\alpha-1} e^{-bt}}{\Gamma(\alpha)} \quad (4)$$

where  $t = x/X_0$ ,  $y = E/E_c$  and  $b \approx 0.5$ ,  $\alpha - 1 = bt_{max}$ , with  $t_{max}$  the point where the distribution has its maximum,

$$t_{max} = 1.0 \cdot (\ln y + C) \quad (5)$$

with values commonly used,  $C=-0.5$  or  $-1.0$  for electrons,  $C=+0.5$  or  $-0.5$  for photons. The energy of the electromagnetic shower is contained at 95% level within distance  $L_{EM}(95\%)$ , which is approximated by

$$L_{EM}(95\%) = X_0 \cdot (t_{max} + 0.08Z + 9.6) \quad (6)$$

The shower develops also in the transverse direction, due to multiple scattering of electrons by nuclei's field (multiple Coulomb scattering). The characteristic length that governs the transverse development of an electromagnetic shower is the so called *Molière radius*,  $R_M$ . It is defined as

$$R_M = X_0 \cdot E_s/E_c \quad (7)$$

where  $E_s = \sqrt{4\pi/\alpha} m_e c^2 = 21.2$  MeV. A simpler approximate expression is  $R_M \approx 7 \cdot A/Z$  (in  $\text{gr}/\text{cm}^2$ ). In general, 90% of shower energy is contained within a cylinder of radius  $R_{EM}(90\%) = R_M$ , 95%(99%) in a radius of  $2 R_M(3.5 R_M)$  respectively.

When the absorber of a calorimeter is a mixture of different elements, the effective radiation length  $X_0$  and Moliere radius  $R_M$  can be calculated with

$$1/X_0 = \sum w_i/X_{0i} \quad \text{and} \quad 1/R_M = \frac{1}{E_s} \sum \frac{w_i E_{ci}}{X_{0i}} \quad (8)$$

where  $w_i$  is the composition by weight and  $X_{0i}$ ,  $E_{ci}$ , the radiation length and the critical energy of the corresponding element.

The total amount of energy ( $E_{visible}$ ) responsible for signal production (scintillation light or charge) is proportional to the total energy loss of shower particles through ionization. Practically  $|dE/dx|_{ion}$  is constant with energy. Thus, the signal that is produced in a calorimeter is proportional to the total track length ( $T$ ) traveled by the charged particles of the shower, hence it is

$$E_{visible} \propto E_{ionization} = T \cdot |dE/dx|_{ion} \propto T \quad (9)$$

Assuming that on average, an electron or a positron interacts through bremsstrahlung after traversing length  $X_0$ , and that a photon converts to a  $e^-e^+$  pair per  $X_0$ , then

after traveling distance  $t = x/X_0$  inside the calorimeter absorber, the shower will consist of  $N = 2^t$  particles, with  $E/N$  energy per particle. Production of new particles stops typically when almost every particle in the shower carries energy around  $E_c$ . Therefore the total particle multiplicity of the shower is roughly equal to  $E/E_c$ , and every particle has traversed distance  $X_0$  on average. Thus, the total track length inside the calorimeter is

$$T = X_0 \cdot E/E_c \quad (10)$$

Equations 9 and 10 clearly manifest the fundamental operation principle of a calorimeter: the produced signal is proportional to the energy of the incident particle.

## 1.2 Hadronic shower development

The incidence of a high energy hadron in a calorimeter [11, 12],[1]-[5] produces a shower of particles due to inelastic collisions with nucleons of the absorber's nuclei. Secondary particles are produced, mainly pions and nucleons, in multiplicity which increases logarithmically with energy per collision. On average 1/3 of the produced pions are  $\pi^0$ 's, that subsequently decay into photons and generate electromagnetic showers. The fraction of the energy of hadrons that does not dissipate in particle production is lost through interactions of excitation of nuclei. Generally this type of interaction does not contribute to signal production.

The characteristic length which governs the longitudinal development of hadronic showers is the *interaction length*,  $\lambda_I$ . In a way similar to the radiation length for electromagnetic showers, it is defined as the mean distance that a hadron traverses to lose  $(1 - 1/e)$  of its energy in inelastic collisions. It is given by

$$\lambda_I = \frac{A}{N_{Av} \cdot \rho \cdot \sigma_{inel}} \text{ cm} \approx 35 \cdot A^{1/3} \text{ gr/cm}^2 \quad (11)$$

where  $A$ ,  $\rho$  is the mass and the density of the material, respectively,  $N_{Av}$  is the Avogadro number and  $\sigma_{inel}$  is the cross section of inelastic interaction for proton.

The longitudinal profile of the energy deposition of a hadronic shower can be parameterized by a sum of a function with the form shown in eq. 4 and a descending exponential, representing the purely electromagnetic and the purely hadronic component of the shower, respectively. From experimental data the maximum of the shower occurs at depth  $t_{max}$ , which is approximately

$$t_{max} \sim 0.2 \ln E + 0.7 \quad (12)$$

with  $t_{max}$  in units of  $\lambda_I$  and  $E$  in GeV. The total depth that is sufficient for 95% containment of the shower energy is

$$L_{had}(95\%) \simeq t_{max} + 2.5 \cdot \lambda_I \cdot E^{0.13}, \quad (E \text{ in GeV}) \quad (13)$$

The transverse development of a hadronic shower is determined by the mean transverse momentum of the produced particles, which is roughly  $\langle p_t \rangle \simeq 0.35$  GeV. The transverse

development does not scale with  $\lambda_I$ , however 95% of the shower energy is contained in a cylinder of radius  $R_{had}(95\%) \lesssim 1 \cdot \lambda_I$ .

The signal that is generated by a hadronic shower is lower than that produced by an electromagnetic one of same energy. This is because a significant fraction, about 25%, 30%, of the total energy dissipated by the hadronic shower inside the calorimeter is lost in nuclear break-up and excitation processes that do not contribute to detectable signal. This intrinsic difference in the response to the two different types of showers is expressed by the *degree of compensation* or *ratio  $e/h$* . This quantity is a characteristic parameter of a calorimeter and is determined by its operation principle and its construction. The  $e/h$  ratio does not depend on energy, it can be derived indirectly by the  $e/\pi$  ratio which is energy dependent. The  $e/\pi$  is the ratio of the signal of an incident electron to the signal produced by the shower of an incident charged pion of same energy. The relation between the two ratios is given by

$$\frac{e}{\pi}(E) = \frac{e/h}{1 + (e/h - 1) \cdot f_{em}(E)} \quad (14)$$

where  $f_{em}(E)$  is defined as the average fraction of energy which contributes to the electromagnetic component of a hadron shower, mainly through  $\pi^0$  production. The  $f_{em}$  function has been studied theoretically and can be approximated by the expressions [13, 14, 23, 15, 16]

$$f_{em}(E) = 1 - \left(\frac{E}{E_o}\right)^{m-1} \quad \text{or} \quad f_{em}(E) = k \cdot \ln\left(\frac{E}{E_o}\right) \quad (15)$$

where  $E_o$ ,  $m$ ,  $k$  are free parameters in the range  $E_o$ : 0.7-1 GeV,  $m$ : 0.8-0.9,  $k$ : 0.1-0.15.

### 1.3 Energy resolution of calorimetric measurement

The development of a shower and the production and collection of its signal are processes with statistical fluctuations, the contributions of which determine the energy resolution of a calorimeter. The number of sources and the amplitude of fluctuations are larger for hadronic showers than for electromagnetic ones, therefore electromagnetic calorimeters show better energy resolution than hadronic ones.

#### Energy resolution for electromagnetic shower

In eq. 10 the total track length of an electromagnetic shower is estimated. We expect the produced signal to be proportional to the total track length. Practically in a calorimeter, only particles with energy greater than a threshold value  $E_{cut}$  ( $\sim 0.5$  MeV) generate detectable signal, thus it is more meaningful to use the total detected track length,  $T_d$ . It is

$$T_d = F(\zeta) \cdot T = F(\zeta) \cdot X_0 \frac{E}{E_c} \quad (16)$$

where the fraction  $F(\zeta)$  is approximated by the formula [5]

$$F(\zeta) \simeq e^\zeta \cdot \left(1 + \zeta \ln\left(\frac{\zeta}{1.526}\right)\right) \quad \text{with} \quad \zeta = 4.58 \frac{ZE_{cut}}{AE_c} \quad (17)$$

In an ideal homogeneous electromagnetic calorimeter of infinite size, without energy leakage, the only source of fluctuations in signal production is the statistical fluctuation of length  $T_d$ , i.e.  $\sigma(E)/E = \sigma(T_d)/T_d$ . This is called *intrinsic fluctuation* because it describes the fluctuation which is related with the fundamental processes that govern the production and development of an electromagnetic shower. Its contribution to the energy resolution is about  $0.7\%/\sqrt{E(\text{GeV})}$ .

$$\left(\frac{\sigma(E)}{E}\right)_{\text{intrinsic}} \simeq \frac{0.7\%}{\sqrt{E(\text{GeV})}} \quad (18)$$

If a fraction of the shower energy leaks out of the calorimeter, then it is

$$\left(\frac{\sigma(E)}{E}\right)_f \simeq \left(\frac{\sigma(E)}{E}\right)_{f=0} \cdot (1 + 4f) \quad (19)$$

where  $f$  is the estimated fraction of energy leakage.

For calorimeters which detect light from scintillation or Cherenkov radiation, statistical fluctuations on the production and collection of photons (*photostatistics*) contribute to the total energy resolution. For low light yield this fluctuation is significant, because the mean number of photoelectrons at photomultipliers per GeV of deposited energy in the calorimeter ( $n_{pe}$ ) is small. It holds  $\sigma_{pe} = \sqrt{n_{pe}}$ , and thus it is

$$\left(\frac{\sigma(E)}{E}\right)_{\text{photostatistics}} = \sqrt{\frac{1}{n_{pe}}} \cdot \frac{1}{\sqrt{E(\text{GeV})}} \quad (20)$$

In sampling calorimeters, in addition to these sources of fluctuations, we also have *sampling fluctuations*. These represent the statistical fluctuations in the number of  $e^-$ 's and  $e^+$ 's that traverse the sensitive material between the absorber layers. If  $d$  is the thickness of each absorber layer and  $T$  the total track length (eq. 10), then the number of tracks that traverse the sensitive material is equal to  $T/d$ . Using instead the total detectable track length,  $T_d$  (eq. 16), the energy resolution reads

$$\left(\frac{\sigma(E)}{E}\right)_{\text{sampling}} \simeq \frac{1}{\sqrt{T_d/d}} = \frac{\sqrt{E_c/F(\zeta)} \cdot \sqrt{d/X_0}}{\sqrt{E}} \quad (21)$$

Using the approximation  $E_c \simeq \frac{550}{Z}$  MeV [5], which has a relative error less than  $\pm 10\%$  for  $13 \leq Z \leq 92$ , and the correction on  $d$  by a factor of  $1/\cos\theta$ , with  $\langle \cos\theta \rangle \simeq \cos\left(\frac{E_s}{\pi E_c}\right)$  to account for the mean angle of the tracks of the shower particles with respect to the direction of the incident particle, we have

$$\left(\frac{\sigma(E)}{E}\right)_{\text{sampling}} \simeq 3.2\% \sqrt{\frac{550}{ZF(\zeta) \cos\left(\frac{E_s}{\pi E_c}\right)}} \cdot \frac{\sqrt{d/X_0}}{\sqrt{E(\text{GeV})}} \quad (22)$$

or equivalently  $\frac{\sigma(E)}{E} \simeq R_{EM} \cdot \frac{\sqrt{d/X_0}}{\sqrt{E(\text{GeV})}}$  with  $R_{EM}$  about equal to 15-20%.



There are also contributions to sampling fluctuations from Landau fluctuations and path length fluctuations [5]. They are negligible for calorimeters with liquid or solid sensitive material, whereas for gaseous calorimeters we should take them into account as they could contribute up to 5% to 10% per  $\sqrt{E}$ .

### Energy resolution for hadronic shower

The intrinsic fluctuations for hadronic showers are large and have a significant contribution to the total energy resolution. This is due to the fact that on average about 1/4 of the energy that is deposited in the calorimeter is dissipated through processes that do not contribute to generation of visible signal. This practically invisible fraction is dominated by large fluctuations, and consequently, the remaining detectable amount of energy shows large fluctuations as well. Besides, the purely electromagnetic component of a hadronic shower is generated mainly by the prompt  $\pi^0$ 's that are produced in the initial interactions. And since the number of  $\pi^0$ 's is small, in approximate it increases logarithmically with energy, it has large statistical fluctuations contributing significantly to the total signal fluctuation. In general, no matter what the calorimeter structure and its operation principle are, the intrinsic fluctuation contribution to the energy resolution for hadronic showers is roughly

$$\left(\frac{\sigma(E)}{E}\right)_{intrinsic} \simeq \frac{45\%}{\sqrt{E(\text{GeV})}} \quad (23)$$

Contributions from energy leakage and photostatistics are approximated by equations 19 and 20, as in the case of electromagnetic showers.

Sampling fluctuations are expected to have similar dependence on absorber layer thickness and on energy as for the electromagnetic showers,

$$\left(\frac{\sigma(E)}{E}\right)_{sampling} \simeq R_{had} \cdot \frac{\sqrt{d/X_0}}{\sqrt{\frac{3}{4} \cdot E(\text{GeV})}} \quad (24)$$

with  $R_{had}$  about 30% to 40% or roughly  $R_{had} \sim 1.5$  to  $2 \cdot R_{EM}$  [5]. The fraction 3/4 expresses the average percentage of the total energy which is deposited in calorimeter through ionization by electrons, positrons and charged hadrons.

As already mentioned, a hadronic shower consists of a purely electromagnetic part and a purely hadronic one, with a relative ratio that depends on the energy of the incident hadron, and which is approximated by the function  $f_{em}(E)$ . The intrinsic difference in the response of a calorimeter to the two different parts of a hadronic shower is expressed by the  $e/h$  ratio. Deviation of  $e/h$  from 1 represents the difference in efficiency to convert the deposited energy to visible signal, depending on the type of particles in the shower. This affects the energy resolution by a constant term, dependent on  $e/h$ ,

$$\left(\frac{\sigma(E)}{E}\right)_{e/h \neq 1} \propto |e/h - 1| \quad (25)$$

by a factor of the order of 15%, 20% [10, 11, 12]. In summary, all non statistical fluctuations contribute to the constant term of the resolution of a calorimeter. Construction defects, material inhomogeneity, calibration errors, non linear response of electronics etc., cause resolution degradation which is difficult to estimate in advance.

## 2 Quartz fiber calorimetry

### 2.1 Motivation

The basic motivation for developing new materials and techniques for detectors is the continuously increasing demands set by the experimental conditions at new accelerators. At the LHC, and also at the heavy ion physics program at SPS and at RHIC, the experimental conditions at forward rapidity regions are very hostile for conventional materials that are used in calorimetry, mainly due to the very high radiation level. Besides, the calorimeters the signal of which is used in high level triggers must have fast response to cope with the high event rate in the experiments. For instance, at the LHC bunch crossing will be every 25 nsec for proton beams, 125 nsec for  $Pb$  beams. Calorimeters with quartz fibers fulfill both requirements of radiation resistance and fast response. First because quartz is a radiation hard material up to Grad level total dose. And second because the operation mechanism of quartz fiber calorimeters is based on the Cherenkov effect, which practically means that the generation and the duration of their signal do not last more than 10 nsec. In the following we discuss in detail the operation principle and the main properties of quartz fiber calorimeters [17]-[35] and [38]-[57], [60, 63, 64, 69].

### 2.2 Principle of operation and Cherenkov effect

The quartz fiber calorimeters are sampling calorimeters. The absorber is made of a dense material such as copper, iron, lead or tungsten and the sensitive medium is composed of quartz fibers. The incident particles interact with the calorimeter's absorber and initiate showers. The charged particles of the shower traversing the optical fibers produce Cherenkov photons, which are guided along the fibers and are collected by photomultipliers. Production of Cherenkov radiation occurs when a charged particle travels in a medium with velocity higher than the velocity of light in that medium. If  $\beta = v/c$  is the velocity of the particle and  $n$  is the index of refraction ( $n=n(\lambda)$ ), then Cherenkov photons are emitted for

$$\beta > \beta_{threshold} = \frac{1}{n} \quad (26)$$

at angle of emission  $\theta_c$ , relatively to the axis of motion of the particle. It holds

$$\cos \theta_c = \frac{1}{n\beta} \quad (27)$$

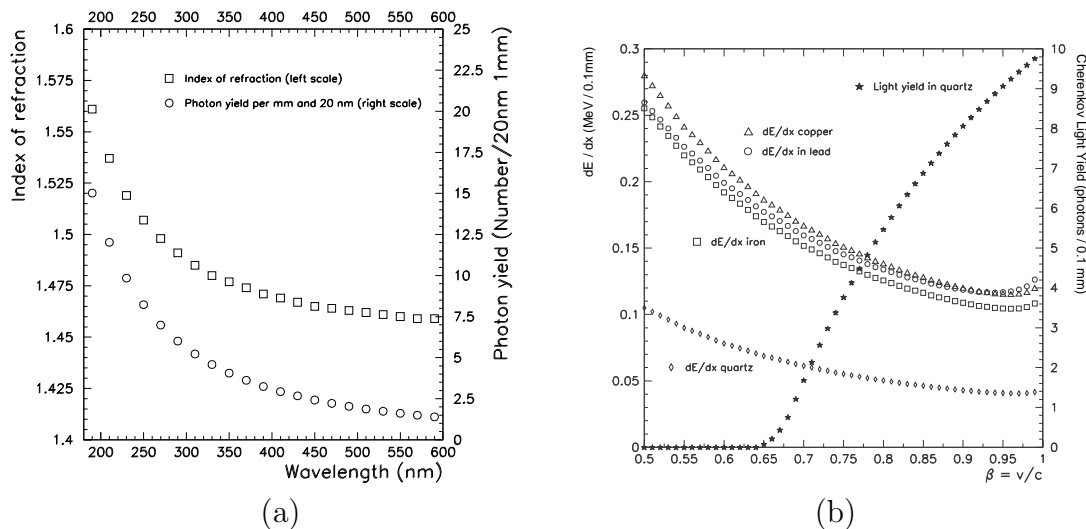


Figure 2: (a) index of refraction of quartz and Cherenkov photon production per unit length as a function of the wavelength, (b) energy loss per unit length from ionization in various materials and Cherenkov photon production per unit length in quartz as a function of the velocity of the incident particle.

The number of photons that are emitted per unit wavelength and per unit path length in the medium is given by the following equation

$$\frac{d^2 N_{ph}}{dL d\lambda} = 2\pi\alpha z^2 \frac{\sin^2 \theta_c}{\lambda^2} = 2\pi\alpha z^2 \frac{1}{\lambda^2} \cdot \left(1 - \frac{1}{n^2\beta^2}\right) \quad (28)$$

where  $\alpha=1/137$ ,  $z$  is the particle charge in units of  $e$ ,  $\lambda$  the wavelength of the photon and  $dL$  the path length in the medium. The emitted light is in the UV part of the spectrum due to the  $1/\lambda^2$  production dependence. It should be noted that the yield of Cherenkov light is 2 to 3 orders of magnitude lower than the yield of scintillation light for the same amount of deposited energy. An intrinsic difference between the two effects is that scintillation light is emitted isotropically, whether Cherenkov light is emitted along a cone with opening angle  $\theta_c$  with respect to the trajectory of the particle. In addition to that, the Cherenkov effect has a production threshold.

Also, it should be emphasized that the Cherenkov effect occurs practically simultaneously ( $< 1$  nsec) with the passage of particles and consequently the width of the produced signal is less than 10 nsec [19, 18, 50, 38].

The index of refraction of quartz is in the range 1.46-1.55, for  $\lambda$  600-200 nm, respectively (see fig. 2(a) from [19] and also eq. 35). Thus, the threshold velocity  $\beta_{threshold}$  is 0.65-0.69 and the angle of emission  $\theta_c$  is  $46^\circ$ - $50^\circ$  for  $\beta \simeq 1$ . In table 1(a) index of refraction, velocity and angle of emission for three different wavelengths are given. In table 1(b) we tabulate the energy required for  $\beta = 0.65$  and  $0.99$  for various charged particles. It results that the minimum kinetic energy that a charged particle should carry to produce Cherenkov light in quartz is 0.33 MeV for electrons and positrons, 119 MeV for pions and 802 MeV for protons.

At this point we would like to remark a characteristic feature of quartz fiber calorime-

Table 1: (a) index of refraction of quartz  $n$ , threshold velocity  $\beta_{threshold}$  and angle of emission of Cherenkov photon  $\theta_c(\beta = 1)$  for various wavelengths, (b) total energy for  $\beta=0.65$  and  $\beta=0.99$  for various charged particles.

(a)				(b)			
$\lambda(\text{nm})$	$n$	$\beta_{threshold}$	$\theta_c$ for $\beta = 1$	particle	mass (MeV)	E(MeV) for $\beta=0.65$	E(MeV) for $\beta=0.99$
200	1.55051	0.645	49.8°	$e^+, e^-$	0.5	0.6	3.5
400	1.46962	0.680	47.2°	$\pi^+, \pi^-$	139.6	183.7	989.6
600	1.45840	0.686	46.7°	$p$	938.3	1234.7	6651.4

ters. From eq. 28, we see that the particles of higher velocities produce more light and so their contribution to the total signal will be larger. In other words this means that a calorimeter which is based on quartz fibers is sensitive mainly to the core of the shower [17, 18, 19, 22, 26] since this part consists of charged particles with relatively larger energies and velocities. On the other hand the calorimeters that are based on  $\frac{dE}{dx}$  technique are mainly sensitive to the charged particles of the shower with lower energies. Consequently the visible transverse size of electromagnetic and hadronic showers in quartz fiber calorimeters is narrower compared to the size of the showers visible by  $\frac{dE}{dx}$  calorimeters.

The main difference between the two types of calorimeters is illustrated in fig. 2(b) (from [19]) which depicts the Cherenkov light yield per unit length (eq. 28) and the energy deposition per unit length ( $dE/dx$  for various absorbers) as a function of particle velocity. It can be clearly seen that the significant part of the signal in conventional calorimeters is contributed by the lower energy particles of the shower since they deposit larger amount of energy. Quartz fiber calorimeters do not collect the deposited energy on fibers but the Cherenkov light emitted inside them by the relativistic charged particles of the shower.

### 2.3 Light propagation in optical fibers

An optical fiber consists of the core, with an index of refraction  $n_{core}$ , and the cladding, with index  $n_{clad}$ . The light propagates inside the fibers due to total internal reflection at the boundary surface of the two elements, and so it must be  $n_{core} > n_{clad}$ . When the light passes from a medium with index of refraction  $n_1$  to a medium with  $n_2$ , it is reflected and refracted. It holds  $\theta_1 = \theta_1'$ ,  $n_1 \sin \theta_1 = n_2 \sin \theta_2$  with  $\theta_1, \theta_1', \theta_2$  the angles between the normal to the boundary surface of the media and the directions of the incident, reflected and refracted light, respectively. The reflection is called internal or external if  $n_1 > n_2$  or  $n_1 < n_2$ , respectively. For  $n_1 > n_2$ , and an incident angle  $\theta \geq \arcsin(n_2/n_1)$  we have reflection only, without refraction. This reflection is called *total internal reflection* and the minimum incident angle required to occur is called *critical angle*. The critical angle for passing from a medium with  $n_1$  to  $n_2$  is

$\theta_{critical}^{1 \rightarrow 2} = \arcsin(n_2/n_1)$ . The so called *lightguide condition* in optical fibers is expressed by

$$\xi \geq \arcsin\left(\frac{n_{clad}}{n_{core}}\right) \quad (29)$$

where  $\xi$  is the angle of incidence of the light to the core-cladding boundary surface. Usually the optical fibers are characterized by the quantity NA, *numerical aperture*, which is defined as

$$NA = \sqrt{n_{core}^2 - n_{clad}^2} \quad (30)$$

From eq. 29 and eq. 30 the lightguide condition can be written as follows

$$\xi \geq \arccos\left(\frac{NA}{n_{core}}\right) \quad \text{or equivalently} \quad \phi = 90^\circ - \xi \leq \phi_{max} \equiv \arcsin\left(\frac{NA}{n_{core}}\right) \quad (31)$$

where  $\phi$  is the angle between the direction of the light and the longitudinal axis of the fiber. For quartz fibers ( $n_{core} \simeq 1.46$ ), the angle  $\phi_{max}$  is  $8.7^\circ$  for NA=0.22,  $14.7^\circ$  for NA=0.37.

The Cherenkov light is emitted inside fibers at a specific angle with respect to the particle direction. The direction dependence of Cherenkov effect combined with the lightguide condition results to the fact that the light output depends on the angle at which the particles traverse the fibers. In fig. 3 [19] is shown a fiber of radius  $R$  traversed by a particle whose track segment is at distance  $b$  from the central axis and at angle  $\alpha$ . At point P, at distance  $\rho$  from fiber's central axis, a Cherenkov photon is emitted and passes through the core-cladding boundary at angle  $\xi$ . We deduce:

$$\cos \xi = \cos \eta \sin \psi \quad (32)$$

with

$$\sin \eta = \frac{\rho}{R} \sin \left( \arctan \frac{\sin \theta_c \sin \omega}{\cos \theta_c \sin \alpha + \cos \omega \sin \theta_c \cos \alpha} + \arcsin \frac{b}{\rho} \right) \quad (33)$$

and

$$\cos \psi = \cos \alpha \cos \theta_c - \sin \alpha \sin \theta_c \cos \omega \quad (34)$$

From equations 32, 33, 34 and the lightguide condition of eq. 31 we have that the production\* of Cherenkov light is maximum for particles traversing the quartz fibers at angles of incidence in the range  $\alpha \pm \Delta\alpha$  with  $\alpha \simeq \theta_c \sim 40^\circ$  to  $50^\circ$  and  $\Delta\alpha \simeq \phi_{max}$ . In fig. 4 [19] the experimental confirmation of this is illustrated [17, 18, 21, 24, 26, 64].

---

\*With production we mean initial production, capture and successful transmission of photons to the edge of fibers in order to be detected and collected as signal.

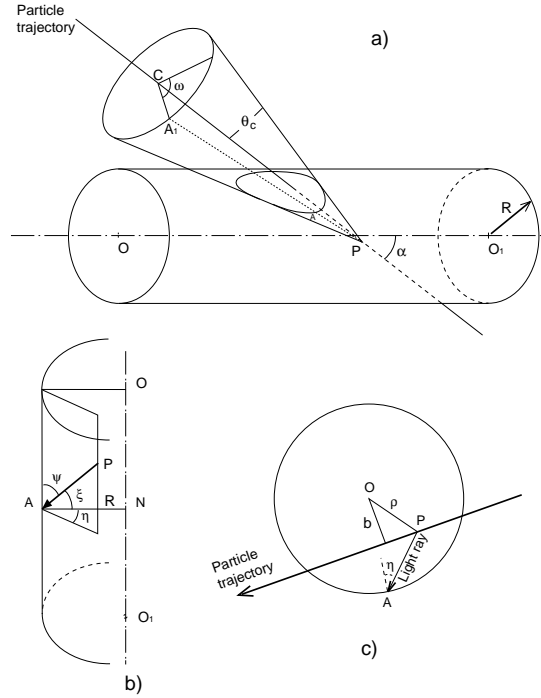


Figure 3: schematic representation of Cherenkov photon production in an optical fiber and illustration of various geometrical parameters.

## 2.4 Quartz optical fibers

The fibers of this type are composed of synthetic fused silica, term commonly used for  $\text{SiO}_2$  in non crystalline state (amorphous material). It is formed by chemical combination of silicon with oxygen in special production process, which provides high purity, level of impurities of the order of 1 part per million. It should not be confused with the fused silica or fused quartz which is a material produced by compression and fusion of crystals of mineral silica. This, besides  $\text{SiO}_2$ , contains oxides of various elements such as  $\text{Fe}_2\text{O}$ ,  $\text{Al}_2\text{O}_3$ ,  $\text{TiO}_2$ ,  $\text{CaO}$ ,  $\text{MgO}$ ,  $\text{Na}_2\text{O}$ . For clarification it should be stressed that by the terms quartz or pure quartz, used often in literature of calorimeters, we mean synthetic fused silica.

Synthetic fused silica has fine optical properties and is widely used in industry of optical systems for producing high quality lenses. It is transparent in a wide range of spectrum, from UV region to IR, has low thermal expansion coefficient ( $\sim 5.5 \cdot 10^{-7}/^\circ\text{C}$ ) and very low coefficient of refractive index change with temperature ( $\sim 1.3 \cdot 10^{-5}/^\circ\text{C}$ ). Its dispersion relation is approximated for  $20^\circ\text{C}$  by the following equation [30], with precision in  $n$  of  $\pm 3 \cdot 10^{-5}$ ,

$$n^2 - 1 = \frac{0.6961663\lambda^2}{\lambda^2 - (0.0684043)^2} + \frac{0.4079426\lambda^2}{\lambda^2 - (0.1162414)^2} + \frac{0.8974794\lambda^2}{\lambda^2 - (9.896161)^2}, \lambda \text{ in } \mu\text{m} \quad (35)$$

The quartz optical fibers are made of core composed of high purity synthetic fused silica or doped with hydroxyl ( $\text{OH}^-$ ) in high ( $\sim 1000$  ppm) or low content ( $\sim 10$  ppm). Their cladding can be composed of quartz doped with fluorine, or is a polymer

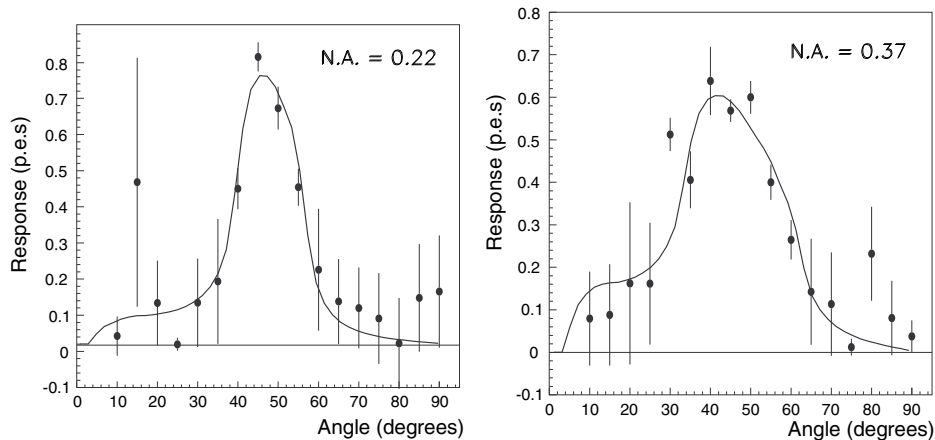


Figure 4: experimental results on the dependence of Cherenkov light production on the angle of the incident particle with respect to fiber's central axis (fibers with NA=0.22 and NA=0.37).

(hard plastic). Quartz fibers are available in core diameters of 200 to 1000  $\mu\text{m}$ , cladding width about 50  $\mu\text{m}$  and numerical aperture NA=0.22, 0.37 or about 0.50. Light of wavelength from  $\sim 200$  nm to  $\sim 1200$  nm is transmitted inside them with attenuation less than 0.05 dB/m, corresponding to an attenuation length  $l_{att} \sim 90$  m. This type of fibers is used in medical and industrial applications, mainly for light transmission or collection in IR.

At this point, it should be also mentioned that quartz, in addition to above properties, is also characterised by extreme resistance to high radiation dose (of the order of 10 Grad) [31], a feature which derives from the strong Si-O chemical bond. Thus the use of fibers with core and cladding composed of quartz (quartz core + fluorine doped quartz cladding) [32, 33, 34, 35] is the only solution for calorimeters that operate in high radiation environment, and in general very hostile conditions for conventional materials. A disadvantage of this type of fibers is their relative high cost. In addition it is a material of high hardness, a feature which makes necessary the use of special shearing methods.

## 2.5 Basic properties of quartz fiber calorimeters

We summarize the basic properties and the main advantages of quartz fiber calorimetry that have been mentioned in previous subsections. The signal in this type of calorimeters is the Cherenkov light which is produced inside the fibers by the traversing charged particles of the shower with  $\beta > \beta_{threshold} \simeq 0.7$ . The fact that for higher particle velocity more Cherenkov photons are emitted, in combination with the directionality of the effect, due to specific angle of emission, and the limitations imposed by the lightguide condition in fibers, make quartz fiber calorimeters be mainly sensitive to the central part of the shower. In other words, the visible transverse width of electromagnetic and hadronic showers is very narrow, in transverse width of about 10 mm and 5-10 cm,

respectively, 95% of the signal is contained [17, 18, 19, 22, 26] and [39, 50, 54, 60, 69]. This size is 3 to 4 times narrower compared to that of calorimeters operating with the  $\frac{dE}{dx}$  technique. This is well illustrated in fig. 5 and 6 [73, 75], which show the part of hadronic shower that a  $\frac{dE}{dx}$  and a quartz fiber based calorimeter is sensitive to, respectively. As a rule of thumb, one can state that the visible part of hadronic showers in quartz fiber calorimeters, and especially for those with 45° fiber inclination geometry, has a transverse development which seems to scale with the Moliere radius and not with the interaction length, as in conventional  $\frac{dE}{dx}$  calorimeters. On the other hand, since the signal of the hadronic showers is produced mainly by their electromagnetic component, the quartz fiber calorimeters are non-compensating ( $e/h > 1$ ).

Another characteristic feature of quartz fiber calorimeters is their very fast response. The Cherenkov effect is an intrinsically fast process which occurs almost simultaneously with the passage of particles. Consequently the duration of signal generation and the signal width do not exceed 10 nsec in time [18, 19, 38, 50].

Using fibers with quartz core and quartz cladding, we can build very radiation hard calorimeters capable to operate up to total dose level of the order of 10 Grad [31, 33, 34, 35].

The main disadvantage of this calorimetric technique is the low light yield, 2 to 3 orders of magnitude lower compared to scintillator based calorimeters for the same amount of deposited energy. To maximize the light production, a geometry with fiber inclination at 45° with respect to the direction of the incident particles is required. With such a configuration a better exploitation of the directionality of the Cherenkov effect and the lightguide condition in fibers is achieved [17, 18, 21, 24, 26, 64]. A 45° inclination geometry sets restrictions and difficulties in construction and is a considerable limitation factor, if we require the calorimeter to provide position measurement as well. Calorimeters with spaghetti structure, where the fibers are embedded inside the absorber volume with a 0° inclination angle with respect to incoming particles, have satisfying light yield for incident particles or jets with energy at the TeV scale. Also, it should be mentioned that quartz fibers are about an order of magnitude more expensive than scintillating fibers, so in general it is not affordable to increase the light production by increasing the filling ratio of the calorimeter.

We conclude this section with table 2, where the main features and properties of quartz fiber calorimetry in comparison with those for  $\frac{dE}{dx}$  method are summarized [17]-[35].

### 3 Quartz fiber calorimeters

The main advantages of quartz fiber calorimeters are, the radiation hardness, to very high dose level (of the order of 1 Grad or more), their fast response ( $< 10$  nsec) and the compact detector dimensions, since the transverse size of the visible shower is very narrow. Calorimeters of this type operate as centrality detectors, trigger detectors, luminosity monitors or calorimeters at very forward regions. In the following subsections we describe the quartz fiber calorimeters that are in operation or under



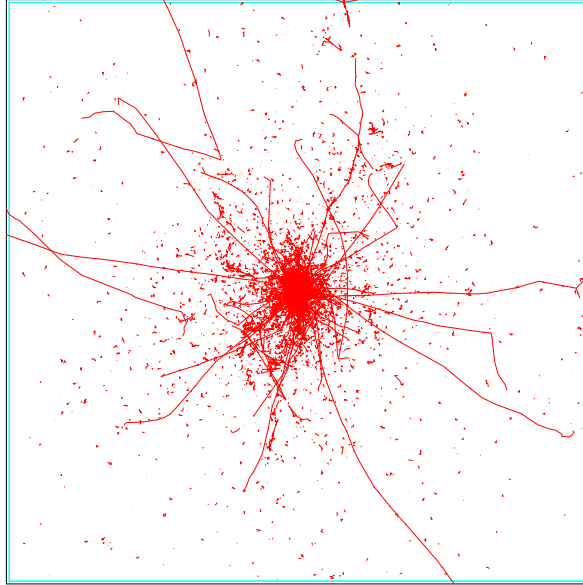


Figure 5: front projected view of a 100 GeV charged pion shower where all charged particle tracks are shown (square size is  $20 \times 20 \text{ cm}^2$ , absorber is W). This is the part of the shower that a  $\frac{dE}{dx}$  based calorimeter is sensitive to.

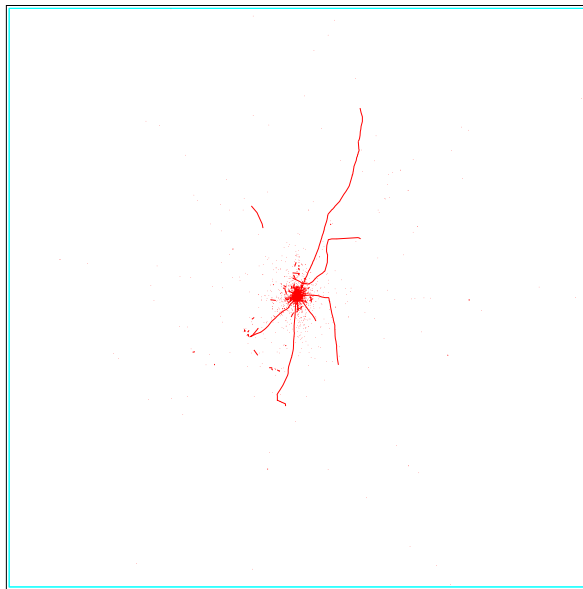


Figure 6: front projected view of a 100 GeV charged pion shower where only tracks of charged particles with  $\beta \geq \beta_{threshold}$  and with direction that gives high probability of Cherenkov photon capture in fibers are shown (square size is  $20 \times 20 \text{ cm}^2$ , absorber is W, fibers with numerical aperture  $NA=0.40$  and  $45^\circ$  inclination). This is the part of the shower that a quartz fiber calorimeter is sensitive to.

Table 2: main features of quartz fiber calorimetry in comparison with  $\frac{dE}{dx}$  calorimetry.

<b>quartz fiber calorimetry</b>	<b><math>\frac{dE}{dx}</math> calorimetry</b>
signal is the Cherenkov light produced in fibers by the charged particles of the shower	signal (light or charge) produced by shower energy deposited in active material
Cherenkov effect has a threshold ( $\beta > \frac{1}{n}$ )	no threshold
non isotropic light emission	light emitted isotropically
sensitive mainly to relativistic charged particles of shower	sensitive mainly to low energy charged particles of shower
intrinsically insensitive to low energy neutrons and to radioactivity	common source of background
detector sensitive to shower core	detector sensitive to total shower
visible transverse size of hadronic shower for 95% signal containment $\mathcal{O}(5-10 \text{ cm})$ , $\mathcal{O}(10 \text{ mm})$ for electromagnetic shower	3 to 4 times wider
light yield $\mathcal{O}(10 \text{ photoelectrons/GeV})$ for $45^\circ$ inclination geometry, $\mathcal{O}(1 \text{ p.e./GeV})$ for $0^\circ$ geometry	$\mathcal{O}(1000 \text{ photoelectrons/GeV})$ for a scintillation based calorimeter
quartz fibers retain their optical properties after total radiation dose of the order of 1 Grad	sensitive materials with considerable degradation of their properties or total destruction to radiation level of 0.01-0.1 Grad
calorimeter capable to operate in very forward rapidity region, in high radiation environment, in high event rate experiments	detector to operate in less demanding conditions

construction/development in various experiments. We first present the calorimeters with fibers placed at  $0^\circ$  inclination with respect to beam axis (“spaghetti” geometry), and then we continue with the ones with  $45^\circ$  construction geometry (“sandwich” structure). The specifications of each calorimeter are tabulated in tables 3 to 9, their main parameters are summarized in tab. 10.

### 3.1 The Zero Degree calorimeter for the NA50 experiment at CERN-SPS

The NA50 [36, 37] is a fixed target experiment of the heavy ion physics research program at CERN-SPS, for detection of matter in quark-gluon plasma phase. The purpose of the experiment is to study the production of vector mesons,  $\rho, \omega, \phi, J/\Psi$  in heavy ion collisions (heavy ion beam on lead target) up to 158 GeV/nucleon beam energy. A quartz fiber calorimeter is used to determine the centrality of the collisions. The calorimeter is placed at 1.6 m after the target, covering pseudorapidity range  $\eta \geq 6.3$  (Zero Degree calorimeter) [38]-[41], [56, 57]. A calorimeter with quartz fibers is imposed by the requirements of tolerance to very high radiation dose expected on the detector site, of the order of 10 Grad, and of fast response, since it provides the trigger signal for the experiment. The calorimeter has a spaghetti structure with fibers embedded in absorber volume at  $0^\circ$  inclination with respect to the beam axis. A brief description of its elements and its main properties is given in table 3. In fig. 7 a general view of the NA50 ZDC is shown.

### 3.2 The Very Forward calorimeter for the CMS experiment at CERN-LHC

The CMS [42] is a collider experiment at the LHC. It will perform Higgs boson and supersymmetric particles research in  $pp$  collisions at  $\sqrt{S_{p+p}} = 14$  TeV. In the very forward region ( $3 \leq |\eta| \leq 5$ ) a calorimeter [43]-[51] with quartz fibers will be used in order to cope with the high radiation and the high event rate requirements of operation. The calorimeter has a spaghetti structure, with fibers embedded in absorber volume at  $0^\circ$  inclination with respect to beam axis. Two identical calorimeters are being built, placed symmetrically in forward and backward regions, and at distance of 11 m from the interaction point. They provide  $2\pi$  azimuth coverage and are segmented in towers with  $\Delta\eta = \Delta\phi = 0.175$ . The specifications of the CMS Very Forward calorimeter are tabulated in table 4, a schematic view is shown in fig. 8.

### 3.3 The Zero Degree calorimeters for the ALICE experiment at CERN-LHC

The ALICE [52] is a heavy ion physics dedicated collider experiment at the LHC. It is designed to search simultaneously for all observables that have been proposed as

characteristic signatures of production of matter in quark-gluon plasma state. It will investigate various systems produced in heavy ion collisions up to a center of mass energy of  $\sqrt{S_{Pb+Pb}} = 1148$  TeV. Zero degree calorimeters that measure the energy of incident neutrons and protons which do not participate in the collision (spectator nucleons) will be used to determine the centrality of the heavy ion collisions. The experimental conditions impose the use of a detector that comprises very fast response, since its signal serves as a trigger signal for the other detectors of the experiment, compact physical dimensions, and high resistance to radiation. These requirements make a quartz fiber calorimeter be the only solution. The ALICE will use two pairs of neutron and proton quartz fiber calorimeters, positioned symmetrically on both sides of the interaction point and at distance of about 115 m [53]-[57]. Both calorimeters have spaghetti geometries, with fibers embedded in absorber at  $0^\circ$  inclination with respect to the beam axis. A brief description of their construction and properties is given in table 5. In fig. 9 a view of the position of the calorimeters between the beam pipes of the LHC is shown.

### 3.4 The Very Forward EM calorimeter for the NA52 experiment at CERN-SPS

The NA52 or NEWMASS [58, 59] was a fixed target experiment at the heavy ion physics program at CERN-SPS. Its objectives included detection of strangelets and study of anti-nuclei production in collisions of  $Pb$  beam on  $Pb$  target, at 158 GeV/nucleon beam energy. A very forward electromagnetic calorimeter [60] was used to measure the energy of photons, produced from  $\pi^0$  decays, in order to determine the centrality of the collision. It was placed at 0.8 m after the target, covering pseudorapidity interval  $2.6 \leq \eta \leq 4.3$ , and  $2\pi$  in azimuth. The calorimeter was equipped with quartz fibers to cope with the high radiation dose expected and for fast response. It consisted of consecutive absorber-fibers layers (“sandwich” geometry) inclined at  $45^\circ$  angle with respect to the beam axis. The calorimeter was also azimuthally segmented in 8 sectors to facilitate studies on anisotropy of transverse energy flow. The main features of the calorimeter are tabulated in table 6, a schematic view is given in fig. 10.

### 3.5 The Zero Degree calorimeters of the experiments at BNL-RHIC

The Relativistic Heavy Ion Collider at BNL provides colliding  $Au$  ion beams at 100 GeV per nucleon ( $\sqrt{S_{Au+Au}} = 39.4$  TeV), lighter ion beams at 125 GeV/nucleon and proton beams at 250 GeV/proton. There are 4 experiments [61, 62] dedicated to the detection and study of the quark-gluon plasma phase. Each experiment is equipped with a pair of identical Zero Degree calorimeters [63, 64], positioned symmetrically on both sides of the interaction point, and at 18 m distance. The calorimeters determine the event centrality and provide triggering signal by measuring the energy of the nucleons that do not participate in the collision. They also operate as luminosity

monitors [65, 66]. Each calorimeter consists of consecutive absorber-fibers layers that are inclined  $45^\circ$  with respect to the beam axis. The specifications of the calorimeters and their schematic views are given in table 7 and depicted in fig. 11, respectively.

### 3.6 The Very Forward EM calorimeter for the H1 experiment at DESY-HERA

The H1 [67, 68] is one of the experiments at the DESY-HERA  $ep$  collider ( $E_e = 27.5$  GeV,  $E_p = 920$  GeV). Its goal is to study the structure of the proton and the properties of its constituents. An electromagnetic calorimeter [69], which measures the energy of photons produced by bremsstrahlung of electrons at the interaction point, is used as a luminosity monitor. The calorimeter has quartz fibers as sensitive material to withstand the radiation level. It consists of consecutive absorber-fibers trapezoid layers with  $45^\circ$  inclination with respect to the beam. A special feature of this calorimeter is that it is also capable to measure the impact point of the incident photons. In particular, this is achieved by alternating fiber planes with horizontal and vertical orientation. Each fiber plane is divided in 12 fiber strips of 10 mm width. The calorimeter signal is read out by 12+12 photomultipliers, for the horizontal and for the vertical set of strips, respectively. With such a configuration, a position resolution of  $\sigma = 5 \text{ mm}/\sqrt{E(\text{GeV})}$  is achieved. The construction parameters and the main properties of the calorimeter are tabulated in table 8. A general view is shown in fig. 12.

### 3.7 The CASTOR calorimeter for the CERN-LHC

The calorimeter is proposed as a very forward detector of the ALICE or CMS experiments at the LHC. Its main objective is to search in the baryon rich, very forward rapidity region of central  $Pb + Pb$  collisions for unusual events, the so called Centauro events, and for “long penetrating objects”, assumed to be strangelets, by measuring the hadronic and electromagnetic energies and the longitudinal profile of the hadronic showers [70]-[75]. It is planned to cover the pseudorapidity range  $5.46 \leq \eta \leq 7.14$ , and  $2\pi$  in azimuth. The calorimeter is azimuthally divided in 8 sectors and longitudinally segmented in consecutive layers of W absorber interleaved with quartz fiber planes having  $45^\circ$  inclination with respect to the beam axis. The calorimeter is composed of a number of channels per sector, read-out by aircore lightguides that will collect and transmit the signal of each channel to its corresponding photomultiplier (see fig. 13) [74, 75]. The specifications and the main properties of the calorimeter are tabulated in table 9. A general view is shown in fig. 13.

### 3.8 Other calorimeters

To the knowledge of the author in order to complete the above list we should also mention the W/quartz fiber polarimeter at the SLD experiment at SLAC and the dual

readout calorimeter R&D project. The former is a calorimeter consisting of sandwiches of tungsten plates and fiber layers with alternating vertical and horizontal orientation to allow position measurement. With a fiducial volume of  $43.5 \times 43.5 \times 115 \text{ mm}^3$  it was capable to measure the energy and the impact point of the Compton scattered photons in order to determine precisely the polarization of the electron beam [76, 77]. In the latter project, a hadronic calorimeter is proposed to be equipped with both scintillating and quartz fibers. A hadron shower generates signals in both materials but by different parts of the shower, as discussed in 2.2 and 2.5. By measuring both signals simultaneously and combining them it is possible to determine the electromagnetic content of hadron showers on an event-by-event basis. This complementary information is then used to correct the energy reconstruction to achieve better response linearity and improve the energy resolution for hadronic showers. First results on this concept with a “spaghetti” geometry prototype can be found in [78].

## 4 Summary

The quartz fiber calorimetry is a technique the signal generation mechanism of which is based on the Cherenkov effect. Namely, the charged particles of the shower with  $\beta > \beta_{threshold}$  when traversing the fibers produce Cherenkov light. The light is captured and lightguided inside the fibers and finally collected by photomultipliers. We described in detail the operation principle and the main properties of this technique and we discussed the quartz fiber calorimeters that have been built or planned to in various experiments. In summary, the advantages of quartz fiber calorimeters are, the radiation hardness, the fast response and the compact detector dimensions. They operate as centrality detectors, trigger detectors, luminosity monitors or general purpose calorimeters at very forward regions.

## Acknowledgements

Many thanks to N. Saoulidou for valuable discussions and comments.

Table 3: specifications of the Zero Degree calorimeter for the NA50 experiment.

<b>purpose</b>	measurement of energy of spectator nucleons (and nuclear fragments) to determine impact parameter of collision and number of participant nucleons
<b>position</b>	1.6 m after the target, covering pseudorapidity range $\eta \geq 6.3$
<b>construction</b>	$5 \times 5 \times 65 \text{ cm}^3$ segmented in 4 towers, depth $5.6 \lambda_I$ , fibers at $0^\circ$ inclination embedded in grooved absorber plates, 1 photomultiplier per tower (total: 4)
<b>absorber</b>	tantalum (Ta: $\lambda_I = 11.5 \text{ cm}$ , $X_0 = 0.4 \text{ cm}$ , density = $16.65 \text{ gr/cm}^3$ ), 30 plates, thickness 1.5 mm each
<b>fibers</b>	pure silica core ( $\varnothing 0.365 \text{ mm}$ ), silica fluorinated cladding, numerical aperture NA=0.22 900 fibers uniformly distributed with 1.5 mm pitch
<b>filling ratio</b>	$\frac{\text{fiber volume}}{\text{absorber volume}} : 1/17 (=5.88\%)$
$\sigma(E)/E$	35(28)% at 100(205) GeV ( $= \frac{2.9}{\sqrt{E(\text{GeV})}} \oplus 19\%$ )
<b>light yield</b>	0.5 photoelectrons per GeV (protons)
<b>total dose</b>	10 Grad

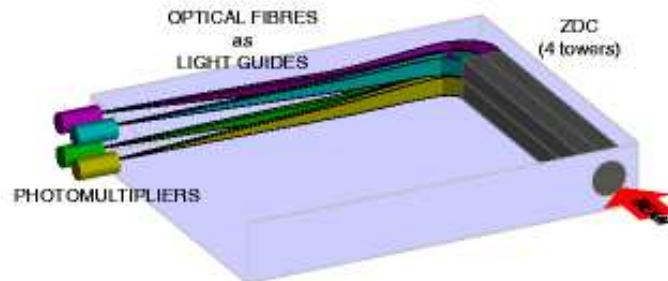


Figure 7: general view of the Zero Degree calorimeter for the NA50 experiment.

Table 4: specifications of the Very Forward calorimeter for the CMS experiment.

<b>purpose</b>	missing energy measurement and forward jet tagging
<b>position</b>	$\pm 11$ m from the interaction point, covering $3 \leq  \eta  \leq 5$ in pseudorapidity and $\phi = 2\pi$ in azimuth
<b>construction</b>	segmented in towers with $\Delta\eta = \Delta\phi = 0.175$ , depth $8.8 \lambda_I$ , fibers at $0^\circ$ inclination embedded in grooved absorber plates 1 photomultiplier per tower (total: 360)
<b>absorber</b>	steel ( $\lambda_I = 17.4$ cm, $X_0 = 1.9$ cm, density = $7.5$ gr/cm <sup>3</sup> )
<b>fibers</b>	quartz core ( $\varnothing$ 0.300 mm), fluorinated doped quartz cladding, numerical aperture NA=0.22
<b>filling ratio</b>	$\frac{\text{fiber volume}}{\text{absorber volume}} < 1\%$
$\sigma(E)/E$	$\frac{2.7}{\sqrt{E(\text{GeV})}} \oplus 13\%$
<b>light yield</b>	$\sim 0.5$ photoelectrons per GeV
<b>total dose</b>	1 Grad

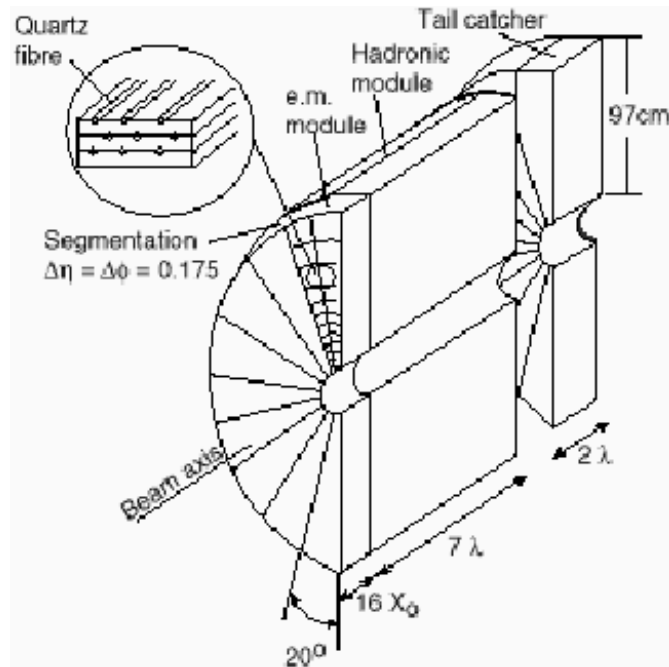


Figure 8: schematic view of one half of the CMS Very Forward calorimeter.



Table 5: specifications of the Zero Degree calorimeters for the ALICE experiment.

	<b>neutron ZDC</b>	<b>proton ZDC</b>
<b>purpose</b>	measurement of spectator neutrons energy for impact parameter determination	measurement of spectator protons energy for impact parameter determination
<b>position</b>	$\pm 116.13$ m from the interaction point	$\pm 115.63$ m from the interaction point
<b>construction</b>	$7 \times 7 \times 100$ cm <sup>3</sup> , depth $8.5 \lambda_I$ , fibers at $0^\circ$ inclination, 5 photomultipliers in total	$20.8 \times 12 \times 150$ cm <sup>3</sup> , depth $8.4 \lambda_I$ , fibers at $0^\circ$ inclination, 5 photomultipliers in total
<b>absorber</b>	W alloy or tantalum (Ta: $\lambda_I = 11.5$ cm, $X_0 = 0.4$ cm, $\rho = 16.65$ gr/cm <sup>3</sup> ), 44 plates 1.6 mm thick each	brass ( $\lambda_I = 18.4$ cm, $\rho = 8.48$ gr/cm <sup>3</sup> ), 52 plates 4 mm thick each
<b>fibers</b>	pure silica core ( $\varnothing 0.365$ mm), silica fluorinated cladding, numerical aperture NA=0.22	pure silica core ( $\varnothing 0.550$ mm), silica fluorinated cladding, numerical aperture NA=0.22
<b>filling ratio</b>	$\frac{\text{fiber volume}}{\text{absorber volume}} : 1/22$ (=4.55%)	$1/65$ (=1.54%)
$\sigma(\mathbf{E})/\mathbf{E}$	10.5% for 2.7 TeV neutrons	$\sim 10\%$ for 2.7 TeV protons
<b>light yield</b>	0.35 photoelectrons per GeV	0.28 photoelectrons per GeV
<b>total dose</b>	$\mathcal{O}(1)$ Grad	$\mathcal{O}(1)$ Grad

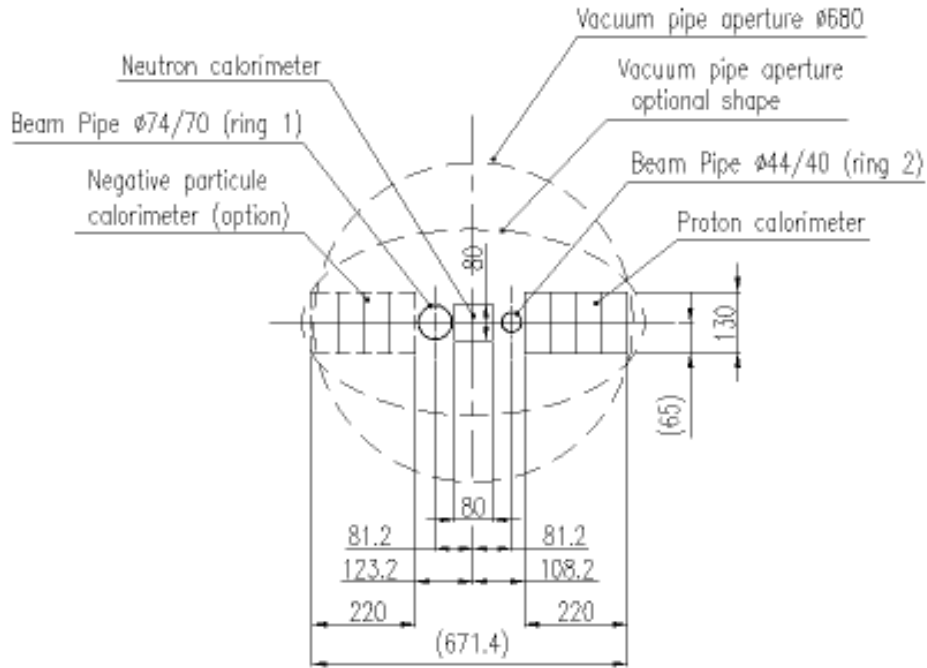


Figure 9: cross section of the LHC beam line and the Zero Degree calorimeters of the ALICE experiment.

Table 6: specifications of the Very Forward Electromagnetic calorimeter for the NA52 experiment.

<b>purpose</b>	photon (from $\pi^0$ decay) energy measurement for impact parameter determination and for studies on transverse energy flow anisotropy
<b>position</b>	0.8 m after the target, covering pseudorapidity $2.6 \leq \eta \leq 4.3$ and $2\pi$ in azimuth
<b>construction</b>	19 consecutive absorber-fibers layers, at $45^\circ$ inclination with respect to beam axis, depth $19 X_0$ , azimuthal segmentation in 8 sectors, 1 photomultiplier per sector (total: 8)
<b>absorber</b>	lead (Pb: $\lambda_I = 17.2$ cm, $X_0 = 0.56$ cm, density = $11.3$ gr/cm <sup>3</sup> ), 19 layers, 4 mm thick each
<b>fibers</b>	quartz core ( $\varnothing$ 0.43 mm), hard plastic cladding, numerical aperture NA=0.22 1 fiber plane per absorber layer
<b>filling ratio</b>	$\frac{\text{fiber volume}}{\text{absorber volume}} : 1/12.8 (= 7.8\%)$
$\sigma(\mathbf{E})/\mathbf{E}$	$\frac{0.56}{\sqrt{E(\text{GeV})}} \oplus 3.6\%$
<b>total dose</b>	1 Grad

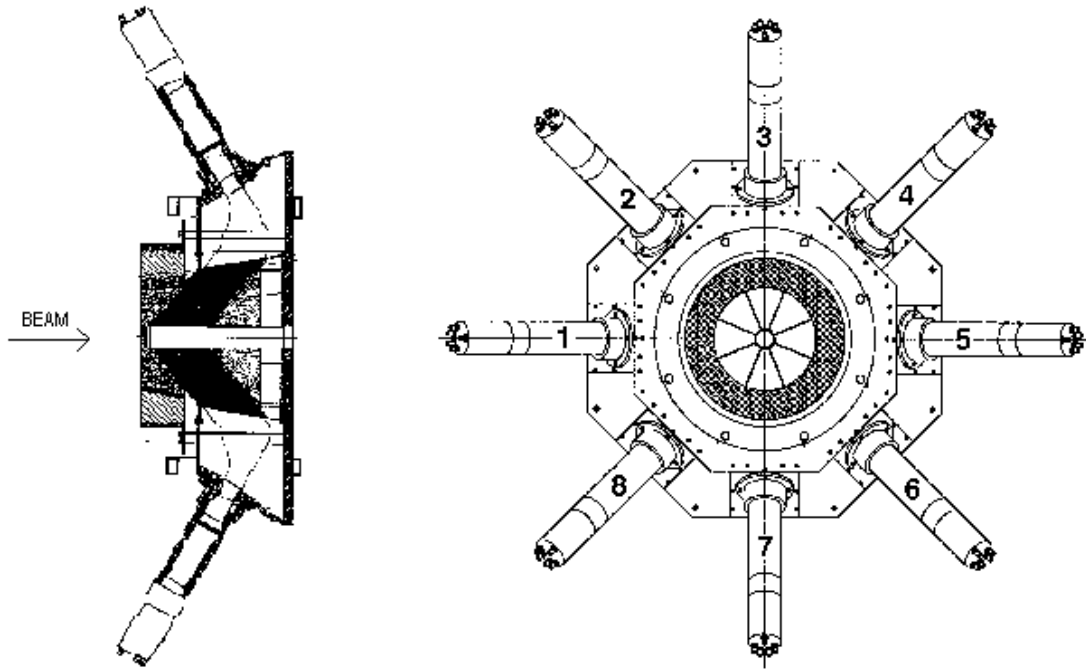


Figure 10: side and front schematic view of the Very Forward Electromagnetic calorimeter for the NA52 experiment.

Table 7: specifications of the Zero Degree calorimeters for the RHIC experiments.

<b>purpose</b>	measurement of spectator neutrons' energy for impact parameter determination and for luminosity monitoring
<b>position</b>	$\pm 18$ m from the interaction point, covering pseudorapidity $ \eta  \geq 6.7$
<b>construction</b>	81 consecutive absorber-fibers layers of $10 \times 18.7$ cm <sup>2</sup> , at 45° inclination with respect to beam axis, depth $5.1 \lambda_I$ , 1 photomultiplier per 27 layers (total: 3)
<b>absorber</b>	tungsten alloy ( $\lambda_I = 11.2$ cm, $X_0 = 0.38$ cm), 81 layers 5 mm each
<b>fibers</b>	PMMA core ( $\varnothing$ 0.45 mm), silica fluorinated cladding ( $\varnothing$ 0.5 mm), numerical aperture NA=0.50 1 fiber plane per absorber layer
<b>filling ratio</b>	$\frac{\text{fiber volume}}{\text{absorber volume}}$ : 8%
$\sigma(\mathbf{E})/\mathbf{E}$	$\frac{0.846}{\sqrt{E(\text{GeV})}} + 9.1\%$ (= 17% at 100 GeV)
<b>light yield</b>	5.2 photoelectrons per GeV (protons)
<b>total dose</b>	100 krad

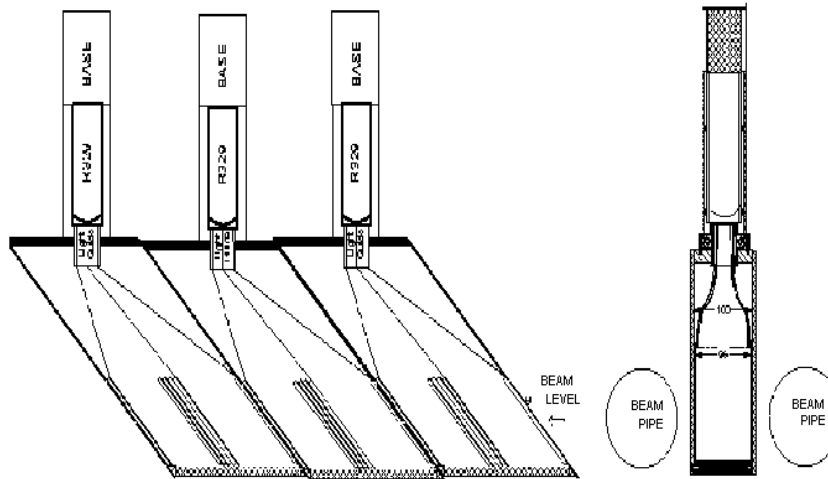


Figure 11: side and front view of the Zero Degree calorimeters for the RHIC experiments.

Table 8: specifications of the Very Forward Electromagnetic calorimeter for the H1 experiment.

<b>purpose</b>	luminosity monitoring by measuring the energy of photons produced by bremsstrahlung of electrons at the interaction point	
<b>position</b>	~100 m from the interaction point	
<b>construction</b>	70 consecutive absorber-fibers layers, at 45° inclination, depth 25 $X_0$ , alternating fiber planes with horizontal and vertical orientation, a fiber plane is divided in 12 strips of 10 mm width each, 12+12 photomultipliers (for horizontal + vertical fiber strips) to determine the x, y impact point of the incident photon	
<b>absorber</b>	tungsten (W: $X_0= 0.356$ cm), 70 layers 0.7 mm thick each	
<b>fibers</b>	quartz core ( $\varnothing$ 0.60 mm), PMMA cladding ( $\varnothing$ 0.64 mm), NA=0.37 1 fiber plane per absorber layer, a fiber plane is divided in 12 strips of 10 mm width each	
<b>filling ratio</b>	$\frac{\text{fiber volume}}{\text{absorber volume}} : 1/1.68 (= 59.5\%)$	
$\sigma(\mathbf{E})/\mathbf{E}$	$\frac{0.19}{\sqrt{E(\text{GeV})}} \oplus 0.5\%$	$\sigma(\text{position}) = \frac{5 \text{ mm}}{\sqrt{E(\text{GeV})}}$
<b>light yield</b>	130 photoelectrons per GeV (electrons)	
<b>total dose</b>	0.1 Grad	

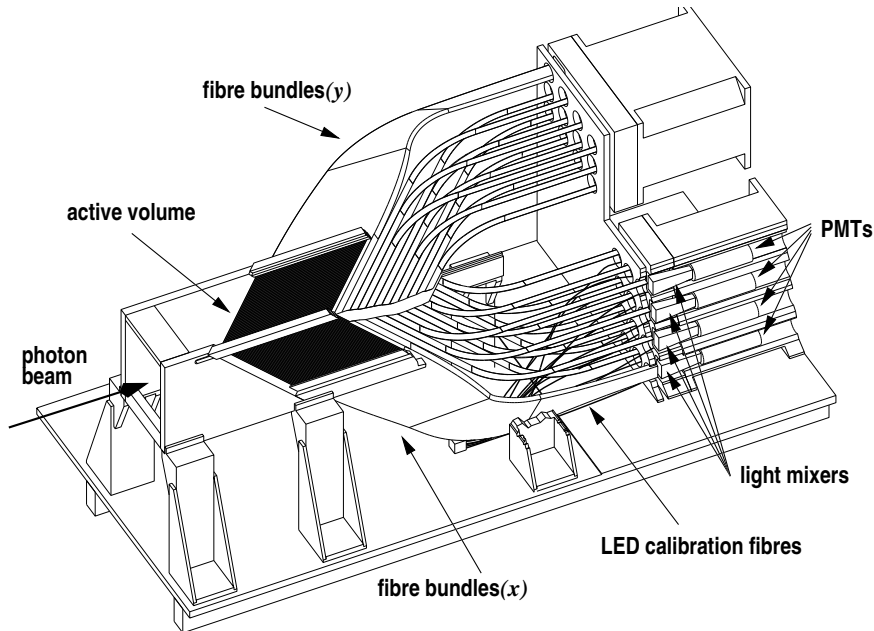


Figure 12: general view of the Very Forward Electromagnetic calorimeter for the H1 experiment.

Table 9: specifications of the CASTOR calorimeter.

<b>purpose</b>	measurement of hadronic and electromagnetic energies and longitudinal profile of hadronic showers in central $Pb + Pb$ collisions
<b>position</b>	16.4 m from the interaction point, covering $5.46 \leq \eta \leq 7.14$ in pseudorapidity and $2\pi$ in azimuth
<b>construction</b>	azimuthal segmentation in 8 sectors, 230 consecutive absorber-fibers layers per sector at $45^\circ$ inclination with respect to beam axis, depth $10 \lambda_I$ 1 lightguide+photomultiplier per $1 \lambda_I$ per sector (total: $8 \times 10$ )
<b>absorber</b>	tungsten (W: $\lambda_I = 10.0$ cm, $X_0 = 0.365$ cm, density = $18.5$ gr/cm <sup>3</sup> ) 230 layers per sector, 0.3 cm thick each ( $d/X_0 = 1.16$ )
<b>fibers</b>	quartz core ( $\varnothing 0.60$ mm), hard plastic cladding ( $\varnothing 0.64$ mm), numerical aperture NA=0.37, 2 fiber planes per absorber layer
<b>filling ratio</b>	$\frac{\text{fiber volume}}{\text{absorber volume}} : 29.5\%$
$\sigma(\mathbf{E})/\mathbf{E}$	$\frac{(21. \pm 0.3)\%}{\sqrt{E(\text{GeV})}} \oplus (0.00 \pm 0.04)\%$ for $e^\pm$ , $\frac{(95. \pm 2.)\%}{\sqrt{E(\text{GeV})}} \oplus (6.5 \pm 0.3)\%$ for $\pi^\pm$
<b>light yield</b>	$\sim 40(30)$ photoelectrons per GeV for $e^\pm(\pi^\pm)$
<b>total dose</b>	$\sim 300$ krad

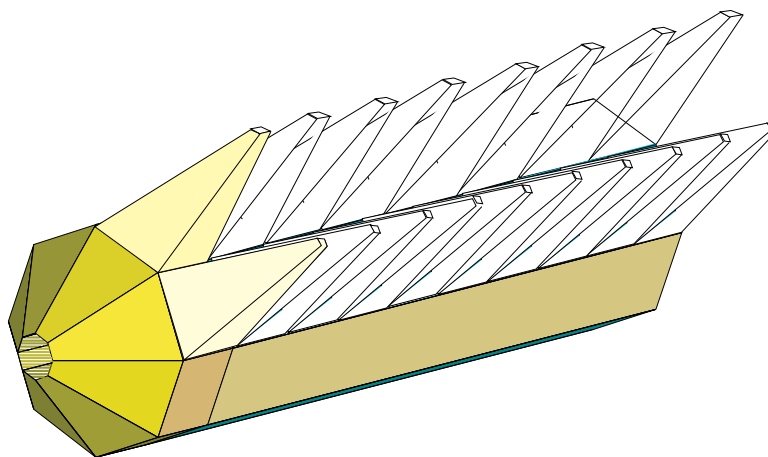


Figure 13: schematic view of the CASTOR calorimeter, some of its aircore lightguides are shown.

Table 10: summary table of the main parameters of the various quartz fiber calorimeters.

calorimeter	geometry	absorber	depth	filling ratio	$\sigma(\mathbf{E})/\mathbf{E}$	light yield	dose
NA50 ZDC	0°	tantalum	5.6 $\lambda_I$	5.88%	$\frac{2.9}{\sqrt{E(\text{GeV})}} \oplus 19\%$	0.5 p.e./GeV	10 Grad
CMS VFCal	0°	steel	8.8 $\lambda_I$	< 1%	$\frac{2.7}{\sqrt{E(\text{GeV})}} \oplus 13\%$	0.5 p.e./GeV	1 Grad
ALICE nZDC	0°	tantalum	8.5 $\lambda_I$	4.55%	10.5% ( $n$ 2.7 TeV)	0.35 p.e./GeV	$\mathcal{O}(1)$ Grad
ALICE pZDC	0°	brass	8.4 $\lambda_I$	1.54%	$\sim 10\%$ ( $p$ 2.7 TeV)	0.28 p.e./GeV	$\mathcal{O}(1)$ Grad
NA52 VFEMcal	45°	lead	19 $X_0$	7.8%	$\frac{0.56}{\sqrt{E(\text{GeV})}} \oplus 3.6\%$		1 Grad
RHIC ZDC	45°	tungsten	5.1 $\lambda_I$	8%	$\frac{0.846}{\sqrt{E(\text{GeV})}} + 9.1\%$	5.2 p.e./GeV	100 krad
H1 VFEMcal	45°	tungsten	25 $X_0$	59.5%	$\frac{0.19}{\sqrt{E(\text{GeV})}} \oplus 0.5\%$	130 p.e./GeV	0.1 Grad
CASTOR	45°	tungsten	10 $\lambda_I$	29.5%	$\frac{0.21}{\sqrt{E(\text{GeV})}} \oplus 0.0\%$ for $e^\pm$ $\frac{0.95}{\sqrt{E(\text{GeV})}} \oplus 6.5\%$ for $\pi^\pm$	40 p.e./GeV for $e^\pm$ 30 p.e./GeV for $\pi^\pm$	300 krad

## References

- [1] P.B.Cushman, *Electromagnetic and hadronic calorimeters*, Instrumentation in High Energy Physics, ed. F.Sauli, World Scientific 1992, Advanced Series on Directions in High Energy Physics, vol.9, p.281
- [2] C.Fabjan, R.Wigmans, *Energy measurement of elementary particles*, Rep.Prog.Phys. 52(1989)1519
- [3] *Experimental techniques in high energy physics*, ed. T.Ferbel, Addison-Wesley 1987
- [4] C.Fabjan, *Calorimetry in high energy physics*, in [3] p.257
- [5] U.Amaldi, *Fluctuations in calorimetry measurements*, Physica Scripta 23(1981)409 and in [3] p.325
- [6] R.Wigmans, *Calorimetry: energy measurement in particle physics*, Oxford University Press 2000
- [7] W.R.Leo, *Techniques for nuclear and particle physics experiments*, Springer-Verlag 1994
- [8] K.Kleinknecht, *Detectors for particle radiation*, Cambridge University Press 1986
- [9] R.C.Fernow, *Introduction to experimental particle physics*, Cambridge University Press 1986
- [10] D.E.Groom *et al.*, Particle Data Group, *Review of Particle Physics*, Eur.Phys.J. C15(2000)1  
K.Hagiwara *et al.*, Particle Data Group, *The Review of Particle Physics*, Phys.Rev. D66(2002)010001
- [11] R.Wigmans, *Advances in hadron calorimetry*, Annual Review of Nuclear and Particle Science 41(1991)133
- [12] R.Wigmans, *On the energy resolution of uranium and other hadron calorimeters*, Nucl.Instr.Meth. A259(1987)389
- [13] D.Acosta *et al.*, *Lateral shower profiles in lead/scintillating fiber calorimeter*, Nucl.Instr.Meth. A316(1992)184
- [14] R.Wigmans *et al.*, *High resolution hadronic calorimetry*, Nucl.Instr.Meth. A265(1988)273
- [15] T.Gabriel *et al.*, *Energy dependence of hadronic activity*, Nucl.Instr.Meth. A388(1994)336
- [16] D.E.Groom, *Energy flow in a hadronic cascade: application to hadron calorimetry*, Proc. of the VII Int.Conf. on Calorimetry in High Energy Physics, (CALOR97) Tucson Nov.1997, ed. E.Cheu *et al.*, World Scientific 1998, p.507
- [17] A.Contin *et al.*, *R&D proposal development of quartz fiber calorimetry*, CERN-DRDC/94-4, 1994
- [18] J.Britz *et al.*, *Status report of the RD40 project*, CERN-LHCC/95-27, 1995
- [19] P.Gorodetzky *et al.*, *Quartz fiber calorimetry*, Nucl.Instr.Meth. A361(1995)161 and CERN-PPE/94-226
- [20] D.Lazic, *Fundamentals of Cherenkov fiber calorimetry*, CERN Yellow Report 97-06 p.86
- [21] M.Lundin *et al.*, *On the electromagnetic energy resolution of Cherenkov-fiber calorimeter*, Nucl.Instr.Meth. A372(1996)359 and CERN-PPE/95-174
- [22] A.Contin *et al.*, *New results in optical fiber Cherenkov calorimetry*, Nucl.Instr.Meth. A367(1995)271
- [23] O.Ganel, R.Wigmans, *Quartz fiber calorimetry for LHC experiments*, Nucl.Instr.Meth. A365(1995)104
- [24] G.Anzivino *et al.*, *Angular dependence of quartz fiber calorimeter response*, Nucl.Instr.Meth. A360(1995)237
- [25] G.Anzivino *et al.*, *Quartz fiber calorimetry - Monte carlo simulation*, Nucl.Instr.Meth. A357(1995)380
- [26] G.Anzivino *et al.*, *Recent developments in quartz fiber calorimetry*, Nucl.Instr.Meth. A357(1995)369
- [27] G.Anzivino *et al.*, *Design of a quartz fiber calorimeter for a collider experiment*, p.462 in Proc. of the 4th Int.Conf. on Calorimetry in High Energy Physics, La Biodola Elba, Sept.1993, eds A.Menzione A.Scribano, World Scientific 1994
- [28] R.Wigmans, *A new approach to forward calorimetry in supercollider experiments*, p.425 in Proc. of the 4th Int.Conf. on Calorimetry in High Energy Physics, La Biodola Elba, Sept.1993, eds A.Menzione A.Scribano, World Scientific 1994
- [29] G.Anzivino *et al.*, *Effects of induced radioactivity in very forward calorimetry*, p.433 in Proc. of the 4th Int.Conf. on Calorimetry in High Energy Physics, La Biodola Elba, Sept.1993, eds A.Menzione A.Scribano, World Scientific 1994

- [30] I.H.Malitson, *Interspecimen comparison of the refractive index of fused silica*, Jour.Optic.Soc. of America 55(1965)1205
- [31] P.Gorodetzky *et al.*, *Very hard radiation resistant and ultra-fast calorimetry*, Radiat.Phys.&Chem. 41(1993)253
- [32] H.Fabian *et al.*, *Producing radiation hard all silica fibers*, CERN Yellow Report 90-10 vol.3 p.736
- [33] V.Gavrilov *et al.*, *Study of quartz fiber radiation hardness*, CMS Technical Note TN-94-324, 1994
- [34] A.D.Avezov *et al.* *Gamma induced transparency loss of thick quartz fibres*, CMS Note 1997/107
- [35] V.Hagopian, *Radiation damage of quartz fibers*, CMS CR 1999/002
- [36] NA50 Collaboration, *Technical Proposal*, CERN/SPSLC 91-55, SPSLC/P 265-Rev
- [37] M.C.Abreu *et al.* (NA50 Collaboration), *Evidence for deconfinement of quarks and gluons from the J/psi suppression pattern measured in Pb-Pb collisions at the CERN-SPS*, Phys.Lett. B477(2000)28
- [38] R.Arnaldi *et al.*, *The quartz-fiber zero-degree calorimeter for the NA50 experiment at SPS*, Nucl.Instr.Meth. A411(1998)1
- [39] E.Chiavassa *et al.*, *A position sensitive highly radiation hard and fast hadron calorimeter for a lead ion experiment at CERN SPS*, Nucl.Instr.Meth. A367(1995)267
- [40] E.Chiavassa *et al.*, *The zero degree hadronic sampling calorimeter for the NA50 experiment at the CERN SPS*, Proc. of the 4th Int.Conf. on Calorimetry in High Energy Physics, La Biodola Elba Sept.1993, eds A.Menzione A.Scribano, World Scientific 1994, p.457
- [41] G.Anzivino *et al.*, *Quartz fibers for very forward calorimetry : ultra-fast, infinitely rad-hard and shower core sensitive*, Proc. of the 4th Int.Conf. on Calorimetry in High Energy Physics, La Biodola Elba Sept.1993, eds A.Menzione A.Scribano, World Scientific 1994, p.438
- [42] CMS Collaboration, *Technical Proposal*, CERN/LHCC 94-38
- [43] Y.Onel, *Present status of CMS HF quartz fiber calorimeter*, Proc. of the 10th Int.Conf. on Calorimetry in Particle Physics, (CALOR2002) CALTECH March 2002
- [44] V.Gavrilov, *CMS quartz fiber calorimeter*, Nucl.Instr.Meth. A453(2000)242
- [45] N.Akchurin *et al.*, *Test beam results of CMS quartz fiber calorimeter prototype and simulation of response to high energy hadron jets*, Nucl.Instr.Meth. A409(1998)593
- [46] N.Akchurin *et al.*, *On the differences between high energy proton and pion showers and their signals in a non-compensating calorimeter*, Nucl.Instr.Meth. A408(1998)380
- [47] J.Merlo, *CMS hadronic forward calorimeter*, Nucl.Phys B(Proc.Suppl) 61B(1998)41
- [48] *The Hadron Calorimeter Project, Technical Design Report*, CERN/LHCC 97-31
- [49] N.Akchurin *et al.*, *Test beam of quartz fiber calorimeter prototype with a passive front section*, Nucl.Instr.Meth. A400(1997)267
- [50] N.Akchurin *et al.*, *Test beam results from a fine-sampling of quartz fiber calorimeter for electron, photon and hadron detection*, Nucl.Instr.Meth. A399(1997)202
- [51] A.Ferrando *et al.*, *A compensating quartz fiber calorimeter for small angle calorimetry at the LHC*, Nucl.Instr.Meth. A390(1997)63
- [52] ALICE Collaboration, *Technical Proposal*, CERN/LHCC 95-71
- [53] *ALICE Zero Degree Calorimeter, Technical Design Report*, CERN/LHCC 99-5
- [54] R.Arnaldi *et al.*, *Performances of zero degree calorimeters for the ALICE experiment*, Nucl.Instr.Meth. A456(2001)248
- [55] R.Arnaldi *et al.*, *The Zero Degree Calorimeters for the ALICE Experiment*, Proc. of the VIII Int.Conf. on Calorimetry in High Energy Physics, (CALOR99) Lisbon Jun.1999
- [56] R.Arnaldi *et al.*, *Quartz fiber ZDCs at CERN SPS and LHC*, Nucl.Instr.Meth. A409(1998)608
- [57] R.Arnaldi *et al.*, *The quartz-fiber calorimeters for the NA50 and ALICE experiments*, Nucl.Phys B(Proc.Suppl) 61B(1998)120
- [58] NEWMASS Collaboration, *Proposal for a Strangelet and Particle search in Pb-Pb collisions, Technical Proposal*, CERN-SPSLC 92-16, SPSLC P268 (1992).



- [59] NA52 Collaboration, *Antinuclei production in heavy ion collisions at CERN SPS*, Nucl.Phys. A661(1999)177c
- [60] M.Weber *et al.*, *A segmented quartz-fiber lead calorimeter*, Proc. of the VII Int.Conf. on Calorimetry in High Energy Physics, (CALOR97) Tucson Nov.1997, ed. E.Cheu *et al.*, World Scientific 1998, p.151
- [61] <http://www.bnl.gov/RHIC>
- [62] W.A.Zajc, *Heavy ion collider detectors*, Nucl.Instr.Meth. A453(2000)25
- [63] RHIC-zdc group, proposal Dec.1998, <http://www.rhic.bnl.gov/~swhite/zcal/>
- [64] C.Adler *et al.*, *The RHIC zero degree calorimeters*, nucl-ex/0008005
- [65] S.N.White, *Forward measurements in RHIC and LHC heavy ion collisions*, Nucl.Instr.Meth. A409(1998)618
- [66] A.J.Baltz *et al.*, *Correlated forward-backward dissociation and neutron spectra as luminosity monitor in heavy ion colliders*, Nucl.Instr.Meth. A417(1998)1, nucl-ex/9801002
- [67] H1 Collaboration, *The H1 detector at HERA*, Nucl.Instr.Meth. A386(1997)310
- [68] H1 Collaboration, *The tracking, calorimeter and muon detectors of the H1 experiment at HERA*, Nucl.Instr.Meth. A386(1997)348
- [69] B.Andrieu *et al.*, *Test beam results of the tungsten/quartz-fibre calorimeter for the luminosity measurement in H1*, Proc. of the IX Int.Conf. on Calorimetry in Particle Physics, (CALOR2000) Annecy Oct.2000, Frascati Physics Series(2001)
- [70] A.L.S.Angelis *et al.*, *Formation and detection of centauro in Pb+Pb collisions at the LHC*, Jour. of Phys. G 28(2002)1937
- [71] A.L.S.Angelis *et al.*, *CASTOR: A forward detector for the identification of Centauro and Strangelets in Nucleus-Nucleus collisions at the LHC*, hep-ex/9901038, hep-ph/9908210
- [72] G.Mavromanolakis *et al.*, *Simulation results on response linearity, energy resolution, and  $e/\pi$  ratio of the CASTOR calorimeter*, ALICE note CAS/2000-20
- [73] G.Mavromanolakis *et al.*, *Simulation results on shower transverse size and response map of the ALICE-CASTOR calorimeter*, ALICE note CAS/2000-25
- [74] G.Mavromanolakis *et al.*, *On the development and design of an aircore lightguide for the ALICE-CASTOR calorimeter*, ALICE note CAS/2000-27
- [75] G.Mavromanolakis, Ph.D. Thesis, University of Athens, 2001
- [76] S.C. Berridge *et al.*, *Quartz fiber/tungsten calorimeter for Compton polarimeter at SLD*, Proc. of the VII Int.Conf. on Calorimetry in High Energy Physics, (CALOR97) Tucson Nov.1997, ed. E.Cheu *et al.*, World Scientific 1998, p.170
- [77] D.V.Onoprienko, Ph.D. Thesis, University of Tennessee, 2000
- [78] R.Wigmans, *First results of the Dual Readout Module (DREAM) project*, Proc. of the XI Int.Conf. on Calorimetry in High Energy Physics (CALOR 2004), Perugia, Mar.2004 and in <http://www.phys.ttu.edu/dream/>